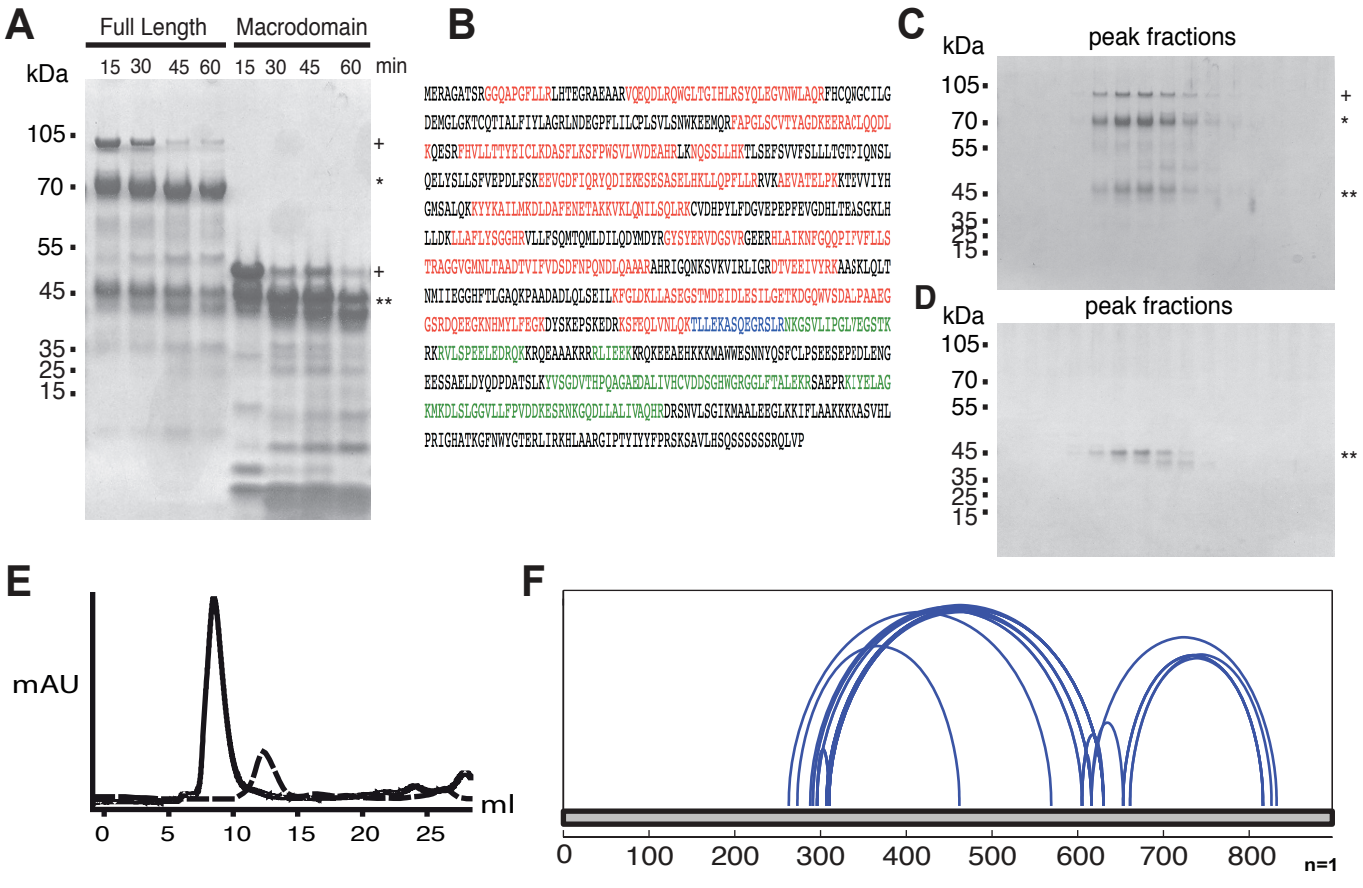

Figure S1. Related to Figure 1. Limited proteolysis identifies two modules within ALC1 and fluorescence-2-hybrid (F2H) assay to probe the interaction of ALC1 ATPase with the macrodomain.

(A) Limited proteolysis of full-length ALC1 (residues 4-897; lanes 1-4) or a macrodomain fragment (570-897; lanes 5-8). Undigested peptides (+) and metastable digestion products are indicated (*, **).

(B) ALC1 sequence indicating the peptides identified using MS fingerprinting. Metastable fragment derived from fl-ALC1 at 70 kDa (*; *red*) and from the macrodomain construct at 35 kDa (**; *green*).

(C) SDS-PAGE showing peak fractions of analytical SEC run of the limited proteolysis sample of full length ALC1.

(D) SDS-PAGE showing peak fractions of analytical SEC run of the limited proteolysis sample of the ALC1 macrodomain.

(E) Overlay of the Superdex S75 10/300 chromatograms corresponding to (c) (*solid line*) and (d) (*dotted line*).

(F) Schematic of ALC1 with the experimentally determined cross-links indicated as arcs. The numbering represents the residue in ALC1.

(G) Setup of the F2H assay. The ratiometric assay quantifies the average fluorescence intensity on the LacO array over the average fluorescence intensity in the nucleoplasm.

(H) Representative images for the negative (vector) controls in our analysis. As expected, no F2H signal is expected for the prey protein.

(I) Quantification of the negative (vector) controls.

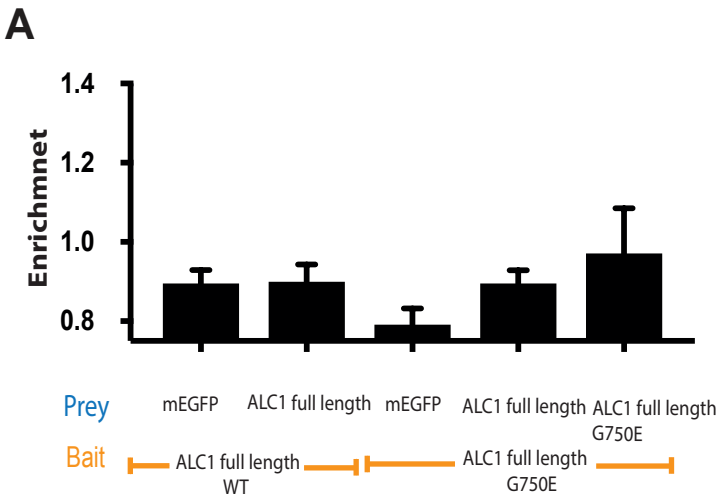

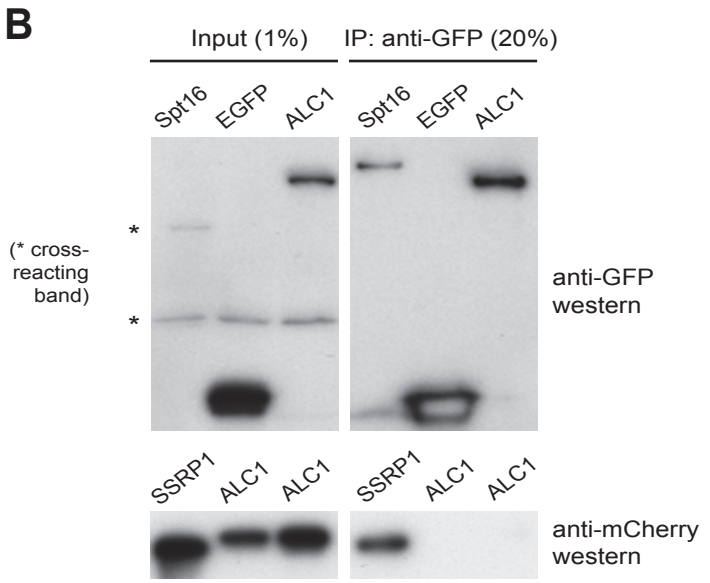

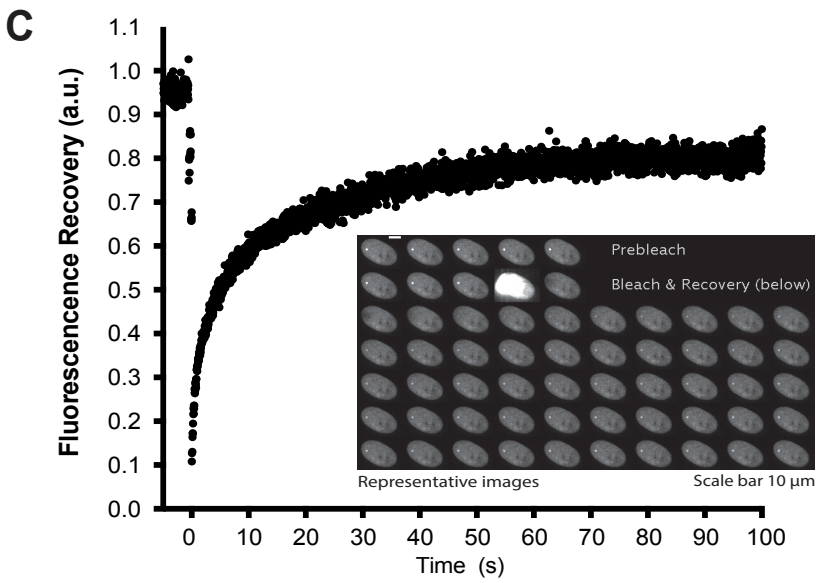

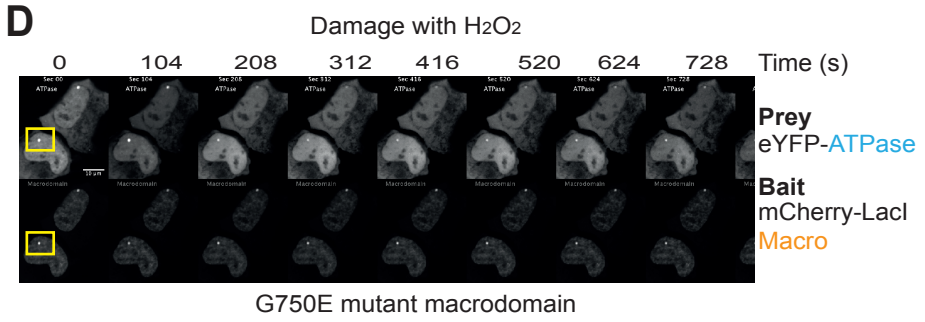

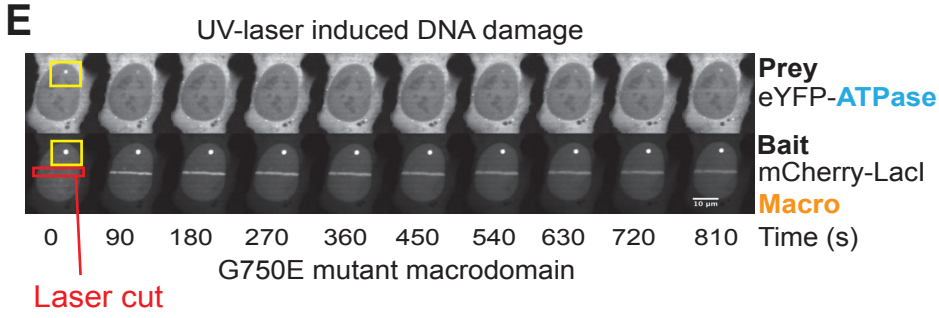

Figure S2. Testing potential inter-molecular interactions between full-length ALC1 and control experiments for some of our life-cell imaging assays.

(A) Related to Figure 1. Fluorescent-2-hybrid (F2H) assay between mCherry-LacI-ALC1 full-length as bait and mEGFP-ALC1 full-length as prey is shown for the indicated constructs. We detect no ALC1–ALC1 interaction, indicating that ALC1 behaves a monomer.

(B) Related to Figure 1. ALC1 does not oligomerize *in vivo*. Co-immunoprecipitation (Co-IP) assays in U2OS cells expressing EGFP- and mCherry-tagged ALC1, EGFP-SPT16 and SSRP1-mCherry (positive control) or EGFP and mCherry-ALC1 (negative control). Cells were treated with 30 µM AG14361 PARP inhibitor for 1 hour prior to lysis to prevent PARP-bridged interactions. GFP-tagged proteins were immunoprecipitated using GFP-TRAP beads and the respective mCherry-tagged interaction partners were detected by western blotting using an mCherry-antibody. We show Co-IP inputs (1% of total) and the IP fractions (20% of total) for the respective Co-IPs.

(C) Related to Figure 2. The Lac repressor bound to LacO array has a fast turnover within the mammalian nucleus. Fluorescence recovery of LacI-mEGFP after photo-bleaching is shown by the fast recovery of the fluorescent Lac repressor in the bleached region. The inset shows the recovery of fluorescence, following the bleaching of fluorescence on the lacO array. LacI-fusions proteins dissociate from their tether on the LacO array, explaining the loss of interaction between the ALC1 ATPase and macrodomain under situations where DNA damage is induced at a site distant from the LacO array (Figure 2A). DNA-damage activated PARP1 (i.e. PARylated PARP1) moves between the site of DNA damage and the LacO array.

(D) Related to Figure 2. Loss of ALC1 ATPase–macrodomain interaction requires the function of the canonical macrodomain ADP-ribose binding pocket. Mutating a key residue (G750) within ALC1's ADP-ribose binding pocket generates a complex that is less sensitive to H_2O_2 induced DNA damage.

(E) Same as (D), but with UV-damage.

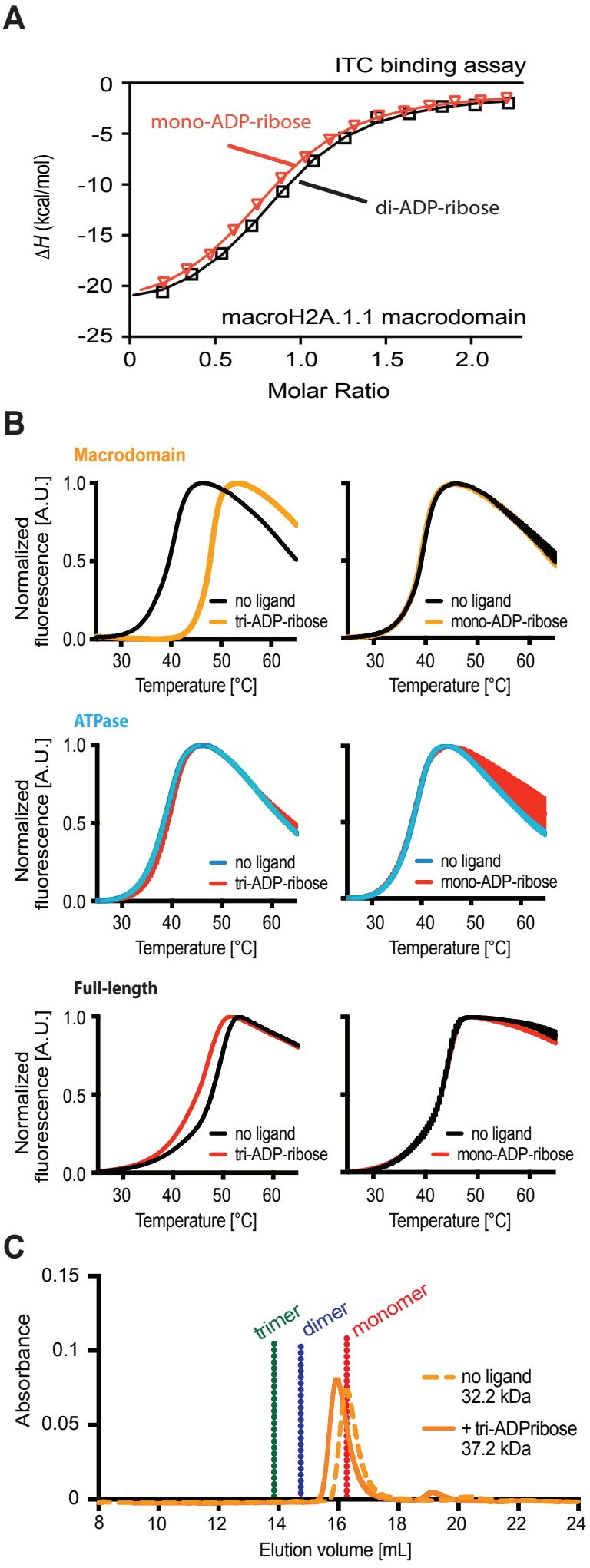

Figure S3. ITC assays, thermal shift analysis and size-exclusion chromatography of macroH2A.1.1 and ALC1 macrodomain modules with monomeric, dimeric and trimeric ADP-ribose.

(A) Related to Figure 3. Unlike for ALC1, the macrodomain of the human MacroH2A.1.1 histone variant binds monomeric ADP ribose and dimeric ADP ribose with the same affinity. Overlap of the ITC titrations for the binding of mono- (*triangles*) and di-ADP-ribose (*squares*) to the macroH2A.1.1 macrodomain.

(B) Related to Figure 3. Thermal-shift analysis reveals strong binding of tri-ADP-ribose to the macrodomain module of ALC1. Fluorescence-based thermal shift assays of full-length ALC1 and individual ALC1 modules in the absence or presence of mono-ADP-ribose and tri-ADP-ribose. *Top, left*: Tri-ADP-ribose stabilizes the ALC1 macrodomain module (residues 636-878) by ~10 °C. *Top, right*: in sharp contrast, monomeric ADP-ribose has no effect on the thermal stability of the ALC1 macrodomain. The isolated ALC1 ATPase module (residues 31-674) remains largely unaffected by the absence or presence of ADP-ribose ligands (*middle*), while the full-length ALC1 protein shows a mild, global decrease of the thermal stability in the presence of tri-ADP-ribose (*bottom, left*), but not in the presence of monomeric ADP-ribose (*bottom, right*). Data shown are representative experiments of technical triplicates (mean +/- SEM).

(C) Related to Figure 3. Size-exclusion chromatography of the ALC1 macrodomain complex in the presand absence of tri-ADP-ribose. Addition of tri-ADP-ribose to the isolated ALC1 macrodomain leads to the earlier elution of the complex, indicating a small increase in the hydrodynamic volume of the ALC1 macrodomain–tri-ADP-ribose complex. However, there is no evidence of tri-ADP-ribose-induced dimerization or trimerization of the ALC1 macrodomain, since dimers and trimers of the ALC1 macrodomain would run earlier in the chromatogram (indicated by the dotted, green trimer and dotted, blue dimer lines).

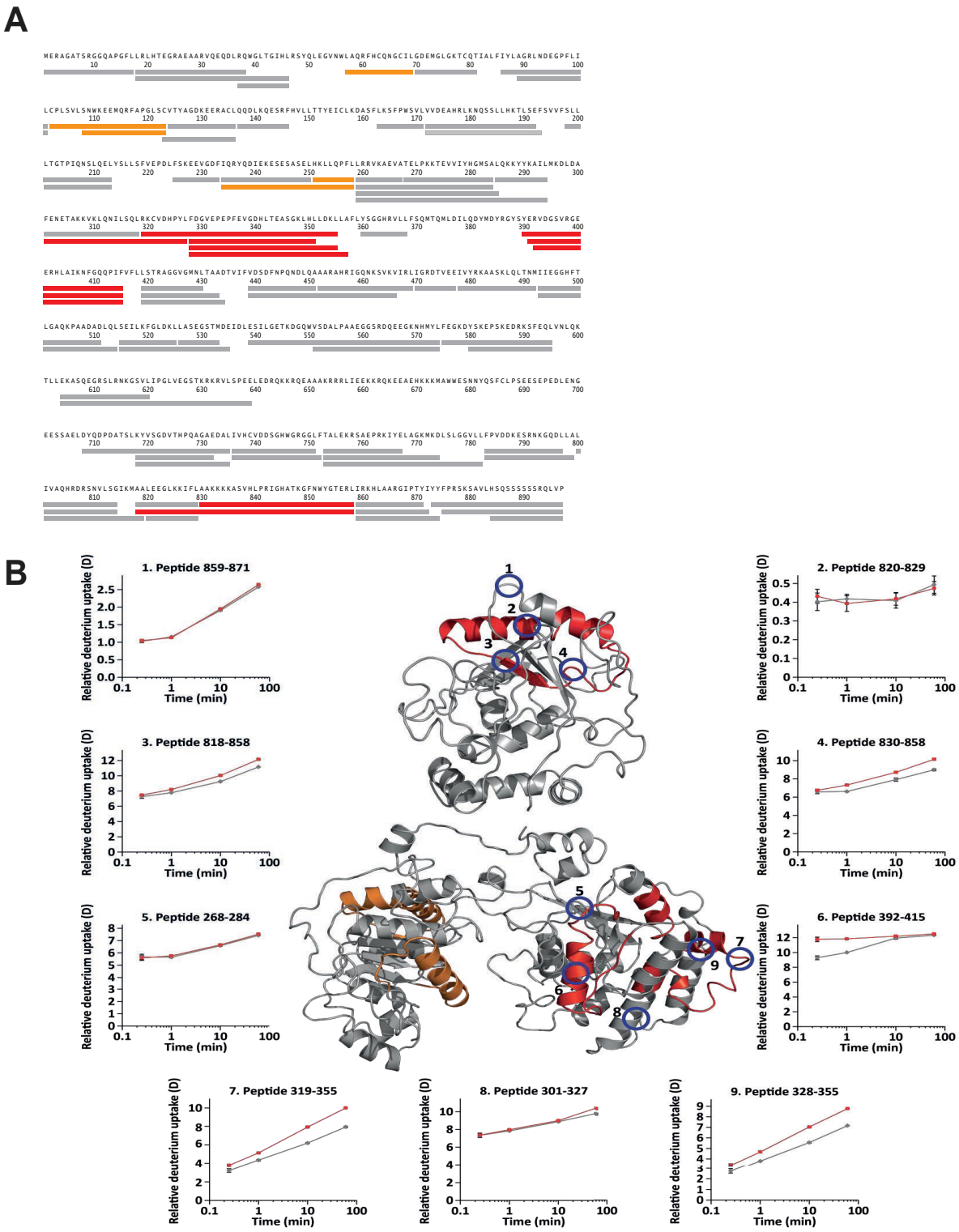

Figure S4. Related to Figure 4. HDX-MS analysis of ALC1 upon binding of tri-ADP-ribose.

(A) HDX-MS peptide coverage map. Regions for which no change in HDX could be observed by MS analysis upon tri-ADP ribose binding (*grey*). Regions undergoing slow unfolding/refolding kinetics (peptides 57-69, 102-123, 108-123, 234-258 and 251-258 (*orange*). Regions showing decreased HDX upon tri-ADP ribose binding (peptide 319-355, 319-358, 328-351, 328-355, 328-357; 390-415, 391-415, 392-415; and 818-858 and 830-858; *red*). (Peptide 301-327 shows changes after 60' incubation).

(B) Highlights of ALC1 peptides whose HDX patterns are changed by tri-ADP-ribose, superimposed on models of the ALC1 macrodomain and ATPase module. Peptides that show a difference in HDX upon addition of tri-ADP ribose are colored red in the macrodomain (*top*, residues 616-897) and ATPase module (bottom, residues 1-615) using I-TASSER structural models. Peptides that exhibit EX1 kinetics are colored in *orange* and peptides that do not show a difference in HDX are colored in *gray*. Deuterium uptake plots show the relative deuterium uptake in individual peptides in upon tri-ADP ribose binding (*red* or *gray* curves, respectively). Deuterium uptake plots numbers 1-4: Deuterium uptake in peptides located within the ALC1 macrodomain. Deuterium uptake plots numbers 5-9: Deuterium uptake in peptides located in the ATPase domain. Peptides 1 and 5 (residues 859-871 and 268-284, respectively) are examples of regions that do not show an effect within their respective domain.

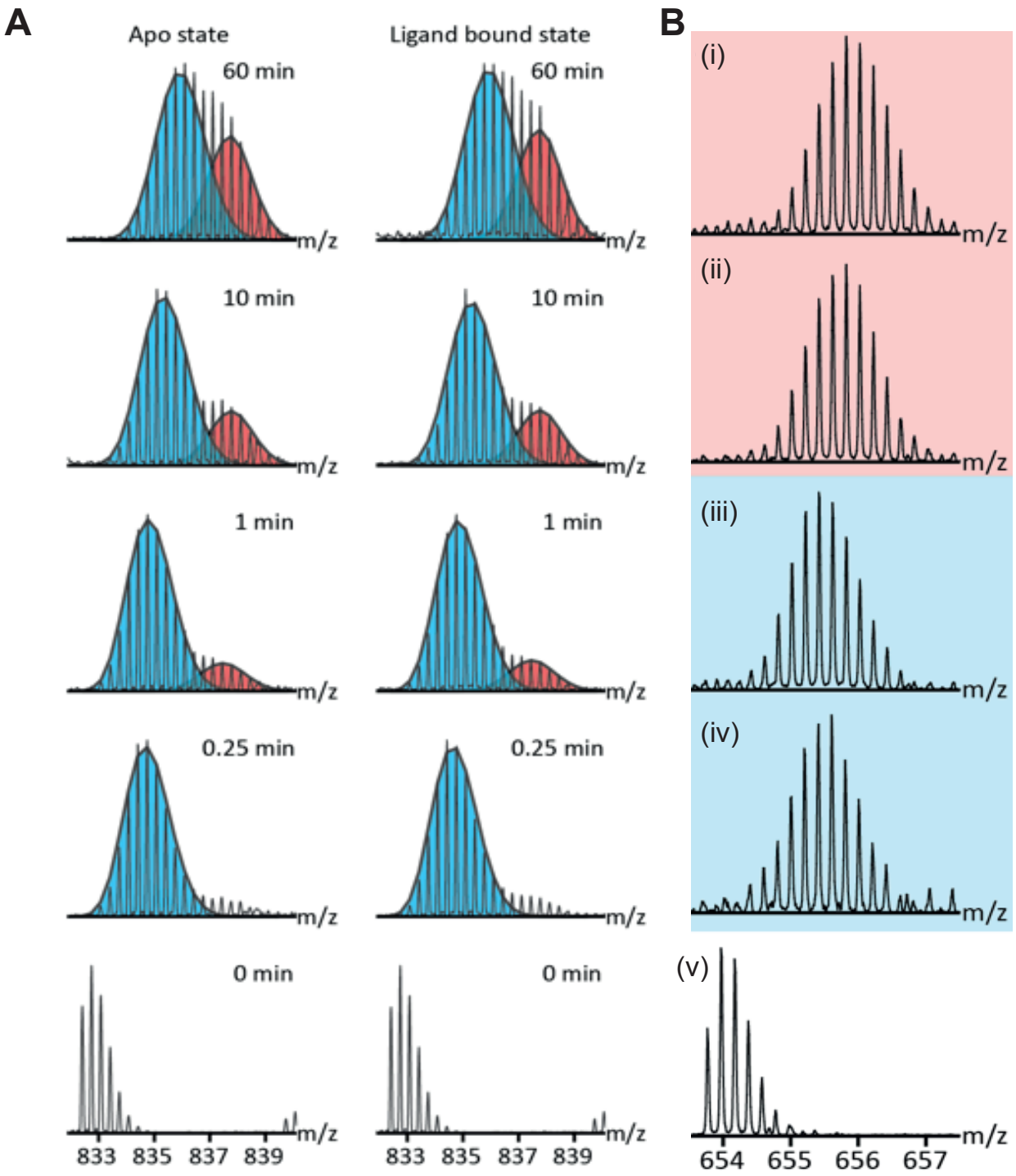

Figure S5. Related to Figure 4. Folding and unfolding kinetics in ALC1 as determined by HDX MS analysis.

(A) Regions in the core Snf2-like chromatin remodeling ATPase domain of ALC1 show slow unfolding/refolding kinetics. Representative spectra of a peptide (residues 102-123) exhibiting slow unfolding/refolding kinetics, referred to as EX1 kinetics, in a region known to participate in the binding and hydrolysis of ATP. We could not observe any different in the rate of unfolding/refolding in the presence (*left*) or in the absence (*right*) of tri-ADP ribose.

(B) In contrast, we do observe Increases in HDX kinetics in the presence of tri-ADP ribose within the ALC1 macrodomain. Representative spectra illustrating increased HDX in a peptide spanning residues 830-858 in the macrodomain: (i) ALC1 incubated for 10 minutes in D_2O-buffer in the presence of tri-ADP ribose; (ii) ALC1 incubated for 10 minutes in D_2O-buffer buffer in the absence of tri-ADP ribose; (iii) ALC1 incubated for 0.25 minutes in D_2O-buffer buffer in the presence of tri-ADP ribose; (iv) ALC1 incubated for 10 minutes in D_2O-buffer buffer in the absence of tri-ADP ribose; (v) Non-deuteriated reference).

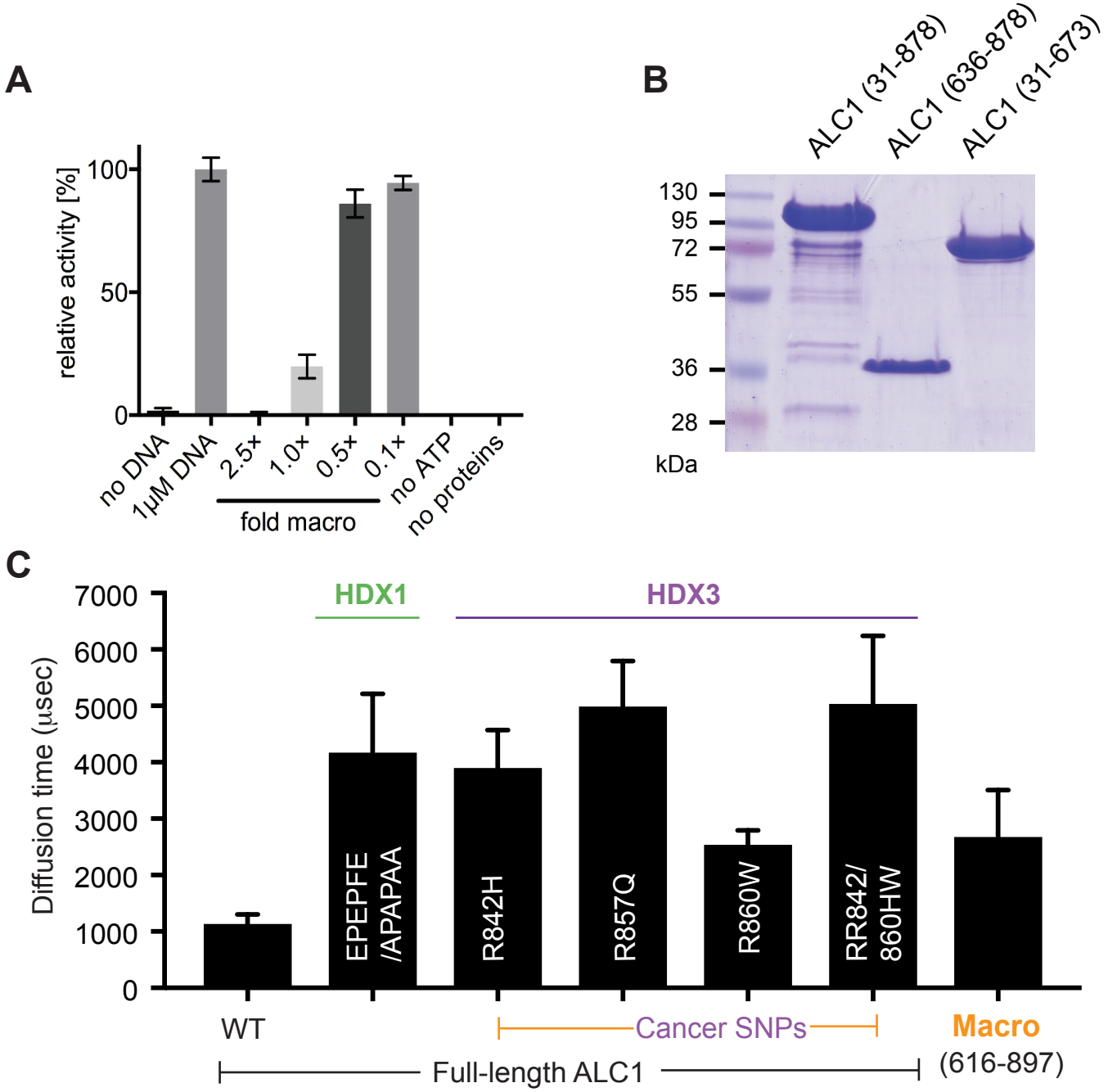

Figure S6. Related to Figure 5. DNA-dependent activity of the ALC1 ATPase module in the presence and absence of the ALC1 macrodomain, and mobility of wild-type and mutant ALC1 proteins in FCS assays.

(A) *In vitro* malachite green ATPase assay of ALC1 using the recombinantly expressed and purified constitutively active ATPase fragment (residues 31-674). The ATPase activity is strictly DNA-dependent. In the absence of DNA, no ATPase hydrolysis can be detected, while 1 µM dsDNA stimulates the ATPase activity. The presence of the ALC1 macrodomain (residues 636-878) inhibits the ATPase in a dose-dependent manner. A 2.5-fold molar excess of the macrodomain over the ATPase module abolishes catalytic activity. Data are normalized to the respective mean value of uninhibited ATPase activity in the presence of 1 µM dsDNA. Omitting ATP or proteins shows that the protein solutions are free of inorganic phosphate contaminations and that no spontaneous ATP hydrolysis occurs under the tested conditions.

(B) Expression and purification of the (near) full-length ALC1 construct (31-878) reveals a number of impurities consisting of fragments of the ALC1 protein, while the recombinant ALC1 ATPase and macrodomain modules purify to very high levels. Likely, ALC1 fragments truncated in the macrodomain display increased relative levels of ATPase activity in the DNA-dependent ATPase assay shown in Figure 3E (left and middle bar).

(C) Fluorescence-correlation-spectroscopy (FCS) assays measure the mobility of wild-type and HDX1/3 mutant ALC1 proteins. Mutations of residues lying within the HDX1 and HDX3 regions of ALC1, including somatic cancer SNPs, affect the mobility of ALC1 inside living nuclei in the absence of exogenous DNA damage. Wild-type ALC1 shows higher mobility compared to HDX1/3 mutant. This raises the possibility that the HDX mutants may show increased DNA/chromatin binding due to the un-gating of the ALC1 chromatin remodeler.

Table S1. Related to Figure 1 and S1. MS-based analysis of intra-molecular crosslinks in the full-length ALC1 protein in the absence of any effector ligand.

List of identified cross-links and identified proteolytic peptides.

Mass (Da)	Charge	Error (ppm)	Score	Peptide 1 sequence	Peptide 2 sequence	Site 1, relative	Site 2, relative	Site 1, absolute	Site 2, absolute
2713.484	4	1.2	6474	KTEVVIYHGMSALQK	IGQNKSVK	1	5	273	462
3256.774	3	2.2	4611	AILMKDLDAFENETAK	VKLQNILSQLR	5	2	296	310
3384.869	4	1.3	13138	AILMKDLDAFENETAK	KVKLQNILSQLR	5	3	296	310
3512.964	5	1.7	1989	AILMKDLDAFENETAK	KVKLQNILSQLRK	5	3	296	310
3543.875	3	0.1	1238	AILMKDLDAFENETAK	NKGSVLIPGLVEGSTK	5	2	296	616
3145.564	4	-0.3	7566	DQEEGKNHMYLFEGK	VKAEVATELPK	6	2	569	263
2413.293	3	2.1	13240	TLLEKASQEGR	YYKAILMK	5	3	605	291
2525.393	3	0	9174	TLLEKASQEGR	KYYKAILMK	5	4	605	291
2966.629	4	0.6	15599	NKGSVLIPGLVEGSTK	TLLEKASQEGR	2	5	616	605
2664.492	5	-0.2	2268	NKGSVLIPGLVEGSTKR	QEAAAKR	2	6	616	653
2681.585	4	2.4	8658	NKGSVLIPGLVEGSTKR	IFLAAKK	2	6	616	832
3046.776	3	4.5	2552	NKGSVLIPGLVEGSTK	VKLQNILSQLR	2	2	616	310
2492.400	3	1.2	10868	NKGSVLIPGLVEGSTKR	KYYK	2	1	616	288
3122.730	4	2	18764	NKGSVLIPGLVEGSTKR	TLLEKASQEGR	16	5	630	605
2960.739	4	2.8	7187	GSVLIPGLVEGSTKR	VKLQNILSQLR	14	2	630	310
3088.834	4	0.7	3319	GSVLIPGLVEGSTKR	KVKLQNILSQLR	14	3	630	310
3088.834	4	0.7	3319	GSVLIPGLVEGSTKRK	VKLQNILSQLR	14	2	630	310
3202.877	4	1	25437	NKGSVLIPGLVEGSTKR	VKLQNILSQLR	16	2	630	310
3271.730	4	1	6590	NKGSVLIPGLVEGSTKR	DLDAFENETAKK	16	11	630	307
3699.976	4	0.6	12096	NKGSVLIPGLVEGSTKR	AILMKDLDAFENETAK	16	5	630	296
2783.572	4	0.5	2573	SNVLSGIKMAALEEGLKK	LIEEKK	8	5	816	661
2797.537	4	0	2337	SNVLSGIKMAALEEGLKK	QEAAAKR	8	6	816	653
2953.638	4	2.6	9596	SNVLSGIKMAALEEGLKK	RQEAAAKR	8	7	816	653
3068.665	4	1.8	4480	DRSNVLSGIKMAALEEGLKK	QEAAAKR	10	6	816	653
1842.134	4	1.9	4616	KIFLAAK	LIEEKKR	1	5	826	661

Table S2. ITC fitting parameters. Related to Figure 3.

Sample	K_D (μM)	Δ*H* (kcal/mol)	Δ*G* (kcal/mol)	-TΔ*S* (kcal/mol)	Stoichiometry (N)	Figure reference
ALC1 macro + **mono**-ADPr	*no binding*	*no binding*	*no binding*	*no binding*	*no binding*	Fig. 3a
ALC1 macro + **di**-ADPr	3.7 (±0.4)	-22.1 (0.5)	-7.4 (±0.1)	14.7 (±0.6)	0.7 (±0.01)	Fig. 3a
ALC1 macro + **tri**-ADPr	10.6 nM (±0.5)	-22.9 (1.5)	-9.7 (±0.1)	13.1 (±1.5)	0.9 (±0.01)	Fig. 3a
ATPase + Macro in the presence of tri-ADP-ribose	*no binding*	*no binding*	*no binding*	*no binding*	*no binding*	Fig. 3c
ATPase + Macro *without* tri-ADP-ribose	0.096 (±0.022)	-22.3 (1.5)	-9.6 (±0.2)	12.7 (±1.6)	1.3 (±0.01)	Fig. 3c
MacroH2A1.1 macro + **mono**-ADPr	1.8 (±0.3)	-19.4 (±3.5)	-7.8 (±0.1)	11.6(±4)	0.9 (±0.10)	Extended Data Fig. 6
MacroH2A1.1 macro + **di**-ADP-ribose	1.1 (±0.1)	-20.8 (±1.3)	-8.1 (0.1)	12.7(±2)	0.9 (±0.03)	Extended Data Fig. 6
Macrodomain + Tri-AAA RNA	*no binding*	*no binding*	*no binding*	*no binding*	*no binding*	*data not shown*
Macrodomain + Tri-A DNA	*no binding*	*no binding*	*no binding*	*no binding*	*no binding*	*data not shown*
Macrodomain + Penta-A DNA	*no binding*	*no binding*	*no binding*	*no binding*	*no binding*	*data not shown*

Abbreviations: ALC1 macro = human ALC1 macrodomain module; ALC1 ATPase = human ALC1 ATPase module; ADPr = ADP-ribose; MacroH2A1.1 macro = macrodomain module of the human histone variant macroH2A.1.1.

Table S3: Oligonucleotides. Related to STAR Methods.

REAGENT or RESOURCE	SOURCE	IDENTIFIER
ATPase assays		
Primer 1	5'-CATGACCAAGTCCAAGCTCCCCAAGCCAGTTCAGGACCTCATC AAGATGATCTTTGGAAGCGGAAGCGGAAGCGGAGGA	N/A
Primer 2	5'-GATCTCCTCCGCTTCCGCTTCCGCTTCCAAAGATCATCTTGAT GAGGTCCTGAACTGGCTTGGGGAGCTTGGACTTGGT	N/A
Cloning		
pmCherry-LacI-C1	FP_BspEI 5'TATATATCCGGACTCAGATCCATGGTGAAACCAGTAACG RP_BglII 5'-TATATAAGATCT.AACCTTCCTCTTCTTCTTAG	N/A
Human SSRP1 mCherry-N1	SSRP1_5_Xho1_1stAS 5'-AATCCGCTCGAGATATGGCAGAGACACTGGAGTTC 203641 SSRP1_3_HindIII_lastAS_nostop 5'-GATCCCAAGCTTCTCATCGGATCCTGACGC	N/A
pmCherry-LacI-ALC1-1-706-C1	L707_stop_FP 5'-GGAAGAGAGCTCTGCTGAGTAGGATTACCAAGACCCAGATGC L707_stop_RP 5'-GCATCTGGGTCTTGGTAATCCTACTCAGCAGAGCTCTCTTCC	N/A
pmCherry-LacI-ALC1-1-673-C1	M674_Stop_FP 5'- GAACATAAGAAAAAGTAGGCCTGGTGGGAATCC M674_Stop_RP 5'-TTAACTGGTATGGTACTGAGGAACTTATTCCGAAACATCTG	N/A
pmCherry-LacI-ALC1-1-614-C1	N615_Stop_FP 5'-CAAGAGGGCCGATCACTCCGATAAAAAGGCAGTGTTCTCATCC N615_Stop_RP 5'-GGATGAGAACACTGCCTTTTTATCGGAGTGATCGGCCCTCTTG	N/A
pEYFP-ALC1-1-614-C1	N615_Stop_FP 5'-CAAGAGGGCCGATCACTCCGATAAAAAGGCAGTGTTCTCATCC N615_Stop_RP 5'-GGATGAGAACACTGCCTTTTTATCGGAGTGATCGGCCCTCTTG	N/A
pET-MCN-ALC1-31-878	5'-CTACCCTCGAGGTGCAGGAGCAGGACTTACGG 5'-AAGGACCAATTGCTAGCTTCTAGGAAAATAATATATG	N/A
pET-MCN-ALC1-31-615	5'-CTACCCTCGAGGTGCAGGAGCAGGACTTACGG 5'-GATGGTCTAGATTAATTTCGGAGTGATCGGCCCTC	N/A
pET-MCN-ALC1-31-605	5'-CTACCCTCGAGGTGCAGGAGCAGGACTTACGG 5'-GATGGTCTAGATTATTTCTCCAAAAGGGTTTTC	N/A
pET-MCN-ALC1-616-876	5'-AGAGGCATATGAATAAAGGCAGTGTTCTCATC 5'-AAGGACCAATTGCTAGCTTCTAGGAAAATAATATATG	N/A
pET-MCN-V5-ALC1-616-876	5'-AGAGGCATATGAATAAAGGCAGTGTTCTCATC 5'-AAGGACCAATTGCTAGCTTCTAGGAAAATAATATATG	N/A
pET-MCN-ALC1-636-876	5'-AGAGGCATATGAGTCCAGAAGAGCTGG 5'-AAGGACCAATTGCTAGCTTCTAGGAAAATAATATATG	N/A
pETM-11 linearization	pETM-11_SLIC F 5'-GACAAGCTTGCGGCCGCACTCGAG pETM-11_SLIC R 5'- GCCCTGAAAATAAAGATTCTCAGTAGTGGGGATGTCG	N/A
Human Spt16	SLIC cloned into EGFP-C1: Spt16 fpEGFPC1 5'-GCTCAAGCTTCGAATTCTGCAGTCGACATGGCTGTGACTCTGG AC Spt16 rpEGFPC1 5'-GATCAGTTATCTAGATCCGGTGGATCCTTACTTCCTCTTTTTCTT	N/A

31-673 into pETM-11 (SLIC)	ALC1 31FpETM11SLIC 5’-CCCACTACTGAGAATCTTTATTTTCAGGGCGTGCAGGAGCAGG ACTTACGG ALC1-3' 673RpETM11SLIC 5’GAGTGCGGCCGCAAGCTTGTCTTACATCTTTTTCTTATGTTCA GCCTCTTCCTTTTGC	N/A
pFBDM-TWINStrep-ALC1-1-897	A1insectfw 5’-GCGCGGTCGACATGGAGCGCGCGG A1insectrev 5’-GCATCGGCGGCCGCTTAAGGCACCAGCTGTCTTG	N/A
Site directed mutagenesis		
pmCherry-C1 Vector	SDM pmCherry-C3 to pmCherry-C1 5’-CGAGCTGTACAAGTCCGGACTCAGATCTCGAGCTC 5’- GAGCTCGAGATCTGAGTCCGGACTTGTACAGCTCG	N/A
G750E	5’-GCCACTGGGGCAGAGGTGAGTTATTTACAGCTCTGGAAAAGC 5’-GCTTTTCCAGAGCTGTAAATAACTCACCTCTGCCCCAGTGGC	N/A
E175Q	5’-GGAGTGTTCTTGTTGTGGATCAGGCTCACAGGTTGAAAAACC 5’-GGTTTTTCAACCTGTGAGCCTGATCCACAACAAGAACACTCC	N/A
EPEPFE/APAPAA	5’-GTTTGATGGTGTGGCTCCGGcTCCTGCTGCAGTTGGAGACCA CCTGACTG 5’-CAGTCAGGTGGTCTCCAACTGCAGCAGGAgCCGGAGCCACAC CATCAAAC	N/A
PEPFE/PAPAA	5'-CAGTCAGGTGGTCTCCAACTGCAGCAGGAGCCGGCTCCACAC CATCAAAC 5'-GTTTGATGGTGTGGAGCCGGCTCCTGCTGCAGTTGGAGACCA CCTGACTG	N/A
RK319/320EE	5'-CATTTTGTCCCAGCTTGAAGAGTGTGTGGATCACCCAT 5'-ATGGGTGATCCACACACTCTTCAAGCTGGGACAAAATG	N/A
K407D	5'-GAGAGACACTTGGCCATTGACAACTTTGGACAGCAGCC 5'-GGCTGCTGTCCAAAGTTGTCAATGGCCAAGTGTCTCTC	N/A
R422E	5'-GTTTTTCTCCTGAGTACTGAGGCAGGTGGAGTTGGCATG 5'-CATGCCAACTCCACCTGCCTCAGTACTCAGGAGAAAAAC	N/A
KK307/308EE	5'-GAAAATGAGACGGCAGAGGAAGTTAAACTACAGAAC 5'-GTTCTGTAGTTTAACTTCCTCTGCCGTCTCATTTTC	N/A
K398E	5'-GTGGATGGTTCTGTGGAAGGAGAAGAGAGACACTTG 5'-CAAGTGTCTCTCTTCTCCTTCCACAGAACCATCCAC	N/A
S420A	5’-CCATTTTCGTTTTTCTCCTGGCTACTAGGGCAGGTGGAGTTGG 5’-CCAACTCCACCTGCCCTAGTAGCCAGGAGAAAAACGAAAATGG	N/A
653-KRRR-656/AAAA	5’-GAAAAGACAAGAAGCAGCTGCCGCGGCAGCGGCACTCATAGA GGAGAAGAAGAGGC 5’-GCCTCTTCTTCTCCTCTATGAGTGCCGCTGCCGCGGCAGCTG CTTCTTGTCTTTTC	N/A
R857E	5’-TTAACTGGTATGGTACTGAGGAACTTATTCCGAAACATCTG 5’-CAGATGTTTCGGAATAAGTTCCTCAGTACCATACCAGTTAA	N/A
R857Q	5'-CTGGTATGGTACTGAGCAACTTATTCGGAAACATC 5'-GATGTTTCCGAATAAGTTGCTCAGTACCATACCAG	N/A
R842H	5'-CAAGTGTTCATCTTCCACATATTGGACATGCCACGAAAG 5'-CTTTCGTGGCATGTCCAATATGTGGAAGATGAACACTTG	N/A
R860W	5'-GGTACTGAGCGACTTATTTGGAAACATCTGGCTGCAAGAG 5'-CTCTTGCAGCCAGATGTTTCCAAATAAGTCGCTCAGTACC	N/A